Fungal lignin peroxidase does not produce the veratryl alcohol cation radical as a diffusible ligninolytic oxidant

Received for publication, December 5, 2017, and in revised form, February 7, 2018 Published, Papers in Press, February 9, 2018, DOI 10.1074/jbc.RA117.001153

Carl J. Houtman[‡], Eranda Maligaspe[‡1], Christopher G. Hunt[‡], Elena Fernández-Fueyo[§2], Angel T. Martínez[§], and Kenneth E. Hammel[‡¶3]

From the [‡]United States Forest Products Laboratory, Madison, Wisconsin 53726, the [§]Centro de Investigaciones Biológicas, Consejo Superior de Investigaciones Científicas, Madrid, Spain, and the [¶]Department of Bacteriology, University of Wisconsin, Madison, Wisconsin 53706

Edited by F. Peter Guengerich

Peroxidases are considered essential agents of lignin degradation by white-rot basidiomycetes. However, low-molecular-weight oxidants likely have a primary role in lignin breakdown because many of these fungi delignify wood before its porosity has sufficiently increased for enzymes to infiltrate. It has been proposed that lignin peroxidases (LPs, EC 1.11.1.14) fulfill this role by oxidizing the secreted fungal metabolite veratryl alcohol (VA) to its aryl cation radical ($VA^{+\bullet}$), releasing it to act as a one-electron lignin oxidant within woody plant cell walls. Here, we attached the fluorescent oxidant sensor BODIPY 581/591 throughout beads with a nominal porosity of 6 kDa and assessed whether peroxidase-generated aryl cation radical systems could oxidize the beads. As positive control, we used the 1,2,4,5-tetramethoxybenzene (TMB) cation radical, generated from TMB by horseradish peroxidase. This control oxidized the beads to depths that increased with the amount of oxidant supplied, ultimately resulting in completely oxidized beads. A reaction–diffusion computer model yielded oxidation profiles that were within the 95% confidence intervals for the data. By contrast, bead oxidation caused by VA and the LPA isozyme of *Phanerochaete chrysosporium* was confined to a shallow shell of LP-accessible volume at the bead surface, regardless of how much oxidant was supplied. This finding contrasted with the modeling results, which showed that if the LP/VA system were to release $VA^{+\bullet}$, it would oxidize the bead interiors. We conclude that LPA releases insignificant quantities of $VA^{+\bullet}$ and that a different mechanism produces small ligninolytic oxidants during white rot.

The oxidative degradation of lignin by white-rot basidiomycetes that decay wood is an important component of global carbon cycling, but remains poorly understood in mechanistic detail. On one hand, there is considerable evidence that specialized peroxidases have an important role. In particular, a subset of them termed lignin peroxidases (LPs)[4] (EC 1.11.1.14) cleaves the principal nonphenolic structures of lignin regioselectively (1–3). Moreover, the LPs, along with structurally related Mn(II)-oxidizing peroxidases (manganese peroxidases, EC 1.11.1.13; and versatile peroxidases, EC 1.11.1.16) are unique to the genomes of most white-rot fungi while being absent from other fungal genomes (1, 4, 5).

On the other hand, many white-rot fungi begin to delignify the wood cell wall before its porosity has increased enough for enzymes to infiltrate, in the process removing lignin faster than they remove polysaccharides (1, 6, 7). This observation of selective delignification suggests that for many fungi the proximal oxidants of lignin, at least during early white rot, are low-molecular-weight agents rather than enzymes. However, the only small oxidants that white-rot fungi indisputably produce are Mn(III) chelates, which are generated by some of the above-mentioned peroxidases but are insufficiently reactive to attack nonphenolic lignin structures (2, 3, 8–10).

It has been proposed that some white-rot fungi circumvent this problem by using LPs to oxidize secreted low-molecular-weight metabolites to reactive-free radicals, which might then diffuse into the wood cell wall and cleave lignin oxidatively (11, 12). LPs are remarkable among peroxidases in their efficient oxidation of aromatic compounds that resemble the major nonphenolic structures of lignin (2), although the versatile peroxidases also have this ability to some extent (8, 9). Substrate oxidation occurs by a classic heme peroxidase mechanism in which compounds I and II of the enzyme catalyze single electron transfers (SETs, Fig. 1) (13), which are mediated by a solvent-exposed tryptophan residue (14–16). When LPs react with nonphenolic lignin structures, the immediate oxidation products are aryl cation radicals that spontaneously fragment between C1 and C2 of the lignin propyl side chain. This oxidative sequence is thought to be the route by which LPs catalyze ligninolysis directly when diffusible mediators are not involved (17, 18).

The chief candidate for a mediator that would operate in conjunction with LP is veratryl alcohol (VA, 3,4-dimethoxy-

This work was supported by United States Department of Energy, Office of Biological and Environmental Research Grant DE-SC0006929 (to K. E. H., C. J. H., and C. G H.). The authors declare that they have no conflicts of interest with the contents of this article.
This article contains Data Set 1, Figs. S1–S4, and Table S1.

[1] Present address: Dept. of Chemistry, St. John's University, Queens, NY 11439.
[2] Present address: Dept. of Biotechnology, Delft University of Technology, 2628 CD Delft, The Netherlands.
[3] To whom correspondence should be addressed: U.S. Forest Products Laboratory, Madison, WI 53726. Tel.: 608-231-9528; Fax: 608-231-9262; E-mail: kehammel@wisc.edu.

[4] The abbreviations used are: LP, lignin peroxidase; SET, single electron transfer; TMB, 1,2,4,5-tetramethoxybenzene; $TMB^{+\bullet}$, 1,2,4,5-tetramethoxybenzene cation radical; VA, veratryl alcohol; $VA^{+\bullet}$, veratryl alcohol cation radical.

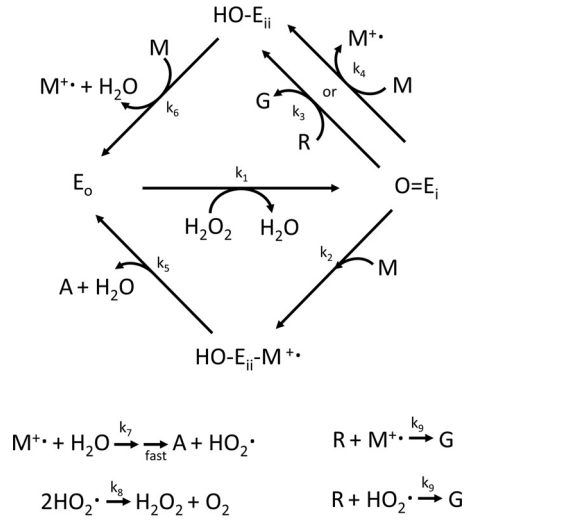

Figure 1. Reactions used for both the reaction–diffusion model and the solution–phase model. The named species are: E_o, ferric resting state peroxidase; O = E_i, two-electron-oxidized peroxidase compound I; HO-E_{ii}, one-electron-oxidized peroxidase compound II; HO-E_{ii}-M$^{+\bullet}$, peroxidase compound II associated with mediator cation radical; M, mediator (TMB or VA); M$^{+\bullet}$, mediator cation radical; A, two-electron-oxidized product derived from mediator (2,5-dimethoxybenzoquinone or veratraldehyde); R, native red BODIPY dye; G, oxidized green BODIPY dye; H_2O_2; and $HO_2^{\bullet}$. Values for the rate constants are given in Table 1.

benzyl alcohol), a secondary metabolite secreted by many white-rot fungi (19). The best-known species is *Phanerochaete chrysosporium*, some isolates of which probably employ low-molecular-weight oxidants because they have been observed to remove lignin from wood faster than they remove cellulose (6). LP oxidizes VA to veratraldehyde (3,4-dimethoxybenzaldehyde) by the same SET mechanism that it employs on nonphenolic lignin structures (13), producing the veratryl alcohol cation radical (VA$^{+\bullet}$) as an intermediate that has been detected by ESR spectroscopy (20). Conceivably, VA$^{+\bullet}$ might escape into solution and then extend the spatial range of LP activity by acting as a SET oxidant of occluded lignin structures (11, 12).

In support of this hypothesis, VA$^{+\bullet}$ is stable enough in water to diffuse several micrometers, hydrolyzing with a rate constant of 17 s^{-1} (11, 21, 22). Furthermore, the oxidation of VA by LP in air at physiological pH (4.5) consumes O_2 and produces ~1.1 veratraldehyde per H_2O_2 supplied (23). This finding suggests that some VA$^{+\bullet}$ may escape oxidation at the LP active site, hydrolyzing instead to give benzylic radicals that rapidly add O_2. The resulting α-hydroxyperoxyl radicals would in turn eliminate the H_2O_2 precursor $HO_2^{\bullet}$, thus accounting for the enhancement in veratraldehyde yield (24). Finally, VA has been shown to enhance some LP-catalyzed oxidations (12, 25–27), and is required for LP to depolymerize colloidal synthetic lignins (28). In some cases, there is good evidence that this stimulation results from mediation by VA$^{+\bullet}$. For example, VA is required for LP to oxidize 4-methoxymandelic acid, which quenches the ESR signal of the VA$^{+\bullet}$ produced, and veratraldehyde production during these reactions occurs only after all of the 4-methoxymandelic acid has been consumed. Moreover, the rate of 4-methoxymandelic acid oxidation by LP exhibits saturation kinetics as the concentration of VA is increased (27).

On the other hand, none of the above observations establish that any of the VA$^{+\bullet}$ produced during LP turnover escapes into free solution. An alternative explanation is that SET from a substrate donor to LP could be mediated by VA$^{+\bullet}$ that remains on the enzyme surface (27, 29). In this case, the physiological and perhaps critically important function of the bound VA$^{+\bullet}$ would be to facilitate contact and electron transfer between the bulky, stereoirregular structures of lignin and oxidized LP, as opposed to acting as a diffusible, remote oxidant of lignin. This concept of VA$^{+\bullet}$ as a bound mediator was introduced because one research group reported that the rate constant for hydrolysis of VA$^{+\bullet}$ is too high for it to diffuse a significant distance (29), and also because chemically generated VA$^{+\bullet}$ failed to oxidize 4-methoxymandelic acid (12). To reconcile these observations with the enzyme kinetics experiments that support mediation, it was hypothesized that a LP–VA$^{+\bullet}$ complex forms during catalysis and is a stronger and more long-lived oxidant that enables the oxidation of recalcitrant substrates (27, 29).

However, VA$^{+\bullet}$ must be able to act as a diffusible oxidant if it is released, because chemically generated VA$^{+\bullet}$ was shown to oxidize a polymeric dye (12). Moreover, multiple studies confirmed that the hydrolysis rate constant for VA$^{+\bullet}$ is in fact relatively low at 17 s^{-1} (11, 21, 22). The problem appears to be that the original research conflated two issues: the redox potential of VA$^{+\bullet}$ and whether LP releases it into solution. Certainly the redox potential of VA$^{+\bullet}$, a dimethoxylated aromatic, is relevant to the oxidation of the monomethoxylated aromatic 4-methoxymandelic acid, whose reaction with VA$^{+\bullet}$ is expected to be thermodynamically unfavorable. However, this constraint does not apply to the oxidation of wood lignin, whose rings carry two or three methoxyl groups, and thus the experiments with 4-methoxymandelic acid and other recalcitrant substrates do not answer the remaining question of whether VA$^{+\bullet}$ can escape the LP active site.

The persistence of this question in the literature, and its importance for our understanding of which small diffusible oxidants white-rot fungi actually employ, led us to conclude that an empirical approach was needed: if some of the VA$^{+\bullet}$ produced by LP can escape the enzyme and oxidize a donor at a distance, then it should be possible to observe the oxidation of a non-recalcitrant substrate immobilized within a porous material that excludes LP (42 kDa) while admitting VA$^{+\bullet}$ (168 Da). As the donor substrate, we used the ratiometric oxidation sensor BODIPY 581/591, which unlike 4-methoxymandelic acid undergoes facile oxidation, and whose fluorescence shifts from red to green once its conjugated diene side chain has been oxidatively cleaved (30). BODIPY 581/591 is directly oxidized by LP, and VA markedly stimulates the reaction by a mechanism not yet determined (31). To make most of the dye inaccessible to direct enzymatic oxidation, we attached it covalently throughout porous polyacrylamide beads that largely exclude LP. In the presence and absence of VA, we treated the beads with LPA, one of the most abundant LP isozymes of *P. chrysosporium* and the only one that has been investigated in mechanistic detail (3, 32). We then used confocal fluorescence microscopy to determine the spatial distributions of BODIPY oxidation in the beads, comparing the results with computer simulations of the profiles expected if free VA$^{+\bullet}$ is the oxidant. In effect, our fluorescent beads serve as a rough model of the similarly semi-porous, lignocellulosic wood cell wall.

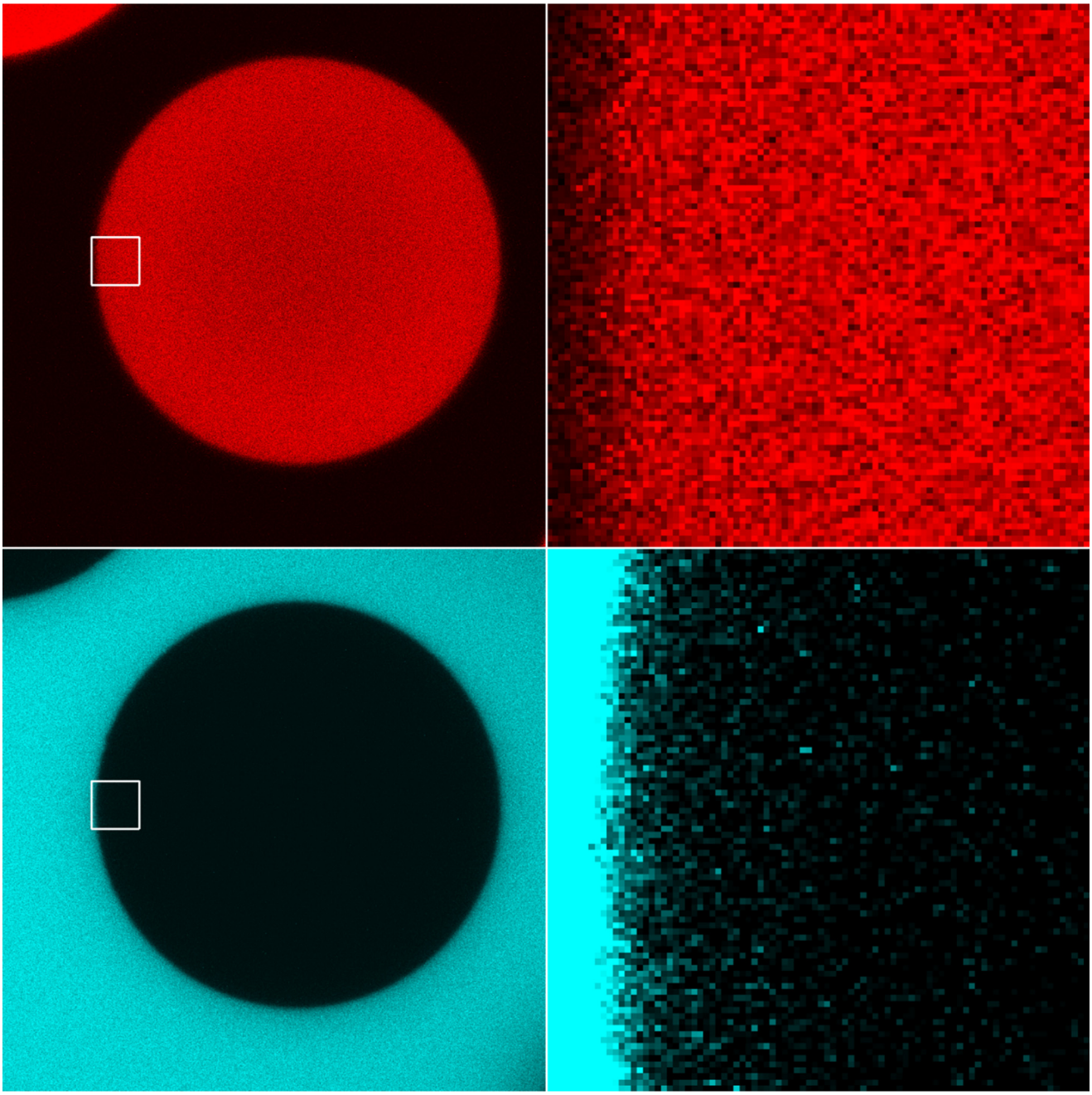

Figure 2. Confocal fluorescence images of a BODIPY-functionalized bead in a solution of fluorescein-labeled ovalbumin. The *red* channel, detecting native nonoxidized BODIPY, is shown at the *top* and the *green* channel, detecting fluorescein, is shown at the *bottom*. The *green* channel is shown in false color (*cyan*) to avoid confusion with the green fluorescence of oxidized BODIPY that appears in the following figures. The *small boxes* in the images on the *left* are 10 × 10 μm in size, and are shown *magnified on the right*.

Results

Properties of dye-functionalized beads

The *upper panels* of Fig. 2 show red channel confocal fluorescence images of a 92-μm diameter polyacrylamide bead containing pores with a nominal 6-kDa molecular mass exclusion, after covalent attachment of BODIPY 581/591 via amide linkages. The distribution of dye throughout the bead is fairly uniform, although a decrease at its center can be discerned. This inhomogeneity in the beads was acceptable for our purposes because the method for measuring dye oxidation is ratiometric, and thus independent of dye concentration.

Close inspection of the bead's edge additionally shows that some BODIPY-labeled polymer extends 1–2 μm into the surrounding solution. The lack of a sharp edge is expected because adsorption of the surfactant used when the beads are manufactured by inverse phase suspension polymerization leads to the formation of larger pores near their surfaces (33, 34). However, this feature leads to an uncertainty of less than 0.25 μm in the position of the edge (see "Experimental procedures").

Before using the beads in oxidation experiments, we made a preliminary estimate of how deeply LPA (42 kDa) could penetrate. This assessment was necessary because beads produced

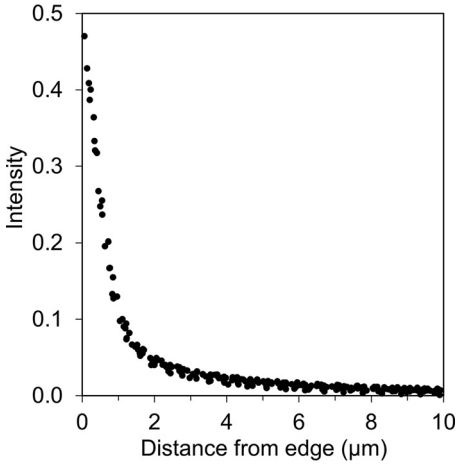

Figure 3. Green fluorescence intensity of BODIPY-functionalized beads when immersed in a solution of fluorescein-labeled ovalbumin. The intensity within the beads is expressed as a fraction of the intensity in the surrounding solution. The data points are from image analyses of nine beads.

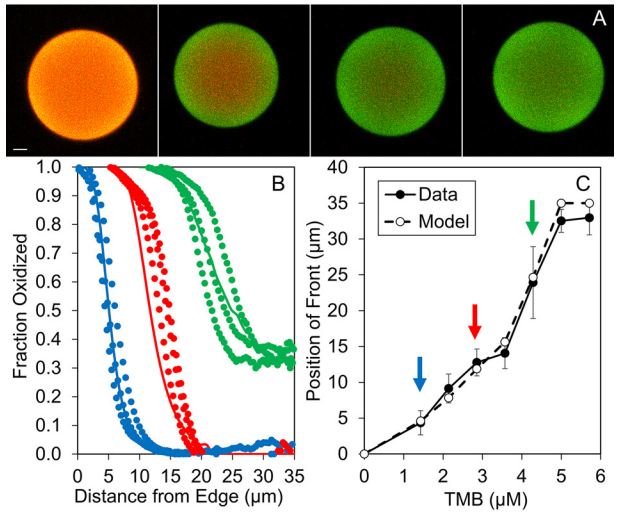

Figure 4. Imaging data for beads treated with peroxidases, TMB, and H_2O_2. *A*, confocal fluorescence images of beads treated with various levels of H_2O_2, using excess TMB (4 mM) and LP. The image sequence, from left to right, is for 0.00, 0.05, 0.10, and 0.40 mM H_2O_2. The images have been adjusted to represent constant excitation laser power. The *scale bar* is 10 μm. *B*, experimental dye oxidation profiles (data points for triplicate beads) and modeled dye oxidation profiles (*lines*) for beads treated with increasing levels of TMB, using excess H_2O_2 (286 μM) and HRP. *Blue*, 1.4 μM TMB; *red*, 2.8 μM TMB; *green*, 4.3 μM TMB. *C*, comparison of experimental data (*closed circles*) and reaction–diffusion model (*open circles*) for the depth into the beads at which 50% oxidation occurred after treatment with the HRP/H_2O_2/TMB system. Results are shown as a function of oxidant dosage, *i.e.* the amount of TMB supplied. *Error bars* on the experimental values indicate 95% confidence intervals. The *colored arrows* indicate the correspondence to the data in plot B.

by inverse phase polymerization do not exhibit an absolute molecular mass exclusion limit, but rather contain a gradient of porosity that decreases from the edge to the core (33, 34). Consequently, the beads were expected to contain a peripheral zone where direct oxidation of the BODIPY by LP could occur without the participation of a diffusible mediator.

To estimate the size of this zone, we suspended beads in a solution of fluorescein-labeled ovalbumin (45 kDa) and obtained both red channel images to visualize the beads (Fig. 2, *upper*) and green channel images to visualize the surrounding solution (Fig. 2, *lower*). A comparison of the images reveals a gradient of green pixels due to fluorescein that diminishes inwards from the edge of the bead. Adjacent to the edge, this green emission appears more intense than it actually is, because the volume sampled by the microscope is not small enough to avoid capturing some of the extremely bright fluorescence from the surrounding solution. However, within the bead the green pixels indicate the presence of the ovalbumin probe.

To quantify this gradient, we conducted image analyses on nine replicate beads. The data are represented as green fluorescence intensity relative to the intensity in the solution surrounding the beads (Fig. 3), and show that 95% of the 45-kDa protein was excluded at a depth of 7 μm. This result suggested that the beads could serve our purpose, provided infiltration of their outermost volume by LP was taken into account.

Proof of principle for mediated bead oxidation

As a test of whether BODIPY 581/591 molecules immobilized within the derivatized beads could detect small, diffusible cation radical oxidants, we began with the oxidation of 1,2,4,5-tetramethoxybenzene (TMB), a synthetic compound that white-rot fungi do not secrete, by LP and by the similarly sized enzyme horseradish peroxidase (HRP, 44 kDa). Both enzymes oxidize TMB to its cation radical ($TMB^{+\bullet}$), which is released into solution and hydrolyzes slowly with a half-life of minutes (35, 36). $TMB^{+\bullet}$ is not only relatively stable, but is also predicted to be a good oxidant with $E^0 = +1.30$ V in H_2O (37). These properties suggest that it could mediate SET oxidations at a distance from the peroxidase from which it was generated.

In preliminary experiments with LP, we exposed the dye-functionalized beads to various levels of H_2O_2 in the presence of excess TMB, waited until spectrophotometric observation at 450 nm showed that $TMB^{+\bullet}$ production had ceased (35, 36), and then examined the beads by confocal fluorescence microscopy. As shown by the representative images of beads in Fig. 4*A*, the initial red emission was replaced from the periphery inwards by green emission, and the beads became entirely green when sufficient H_2O_2 had been added. Our supply of LP being limited, we then performed a larger number of quantitative experiments using HRP, exposing the beads to various levels of TMB in the presence of excess H_2O_2. This experiment revealed the presence of a distinct advancing front of oxidation that progressed toward the bead center as a function of the amount of $TMB^{+\bullet}$ supplied (Fig. 4*B*), which established that our beads were a suitable reporter for small aryl cation radical oxidants.

Development of a reaction–diffusion model

We next developed a mathematical model for bead oxidation and checked its validity against the experimental results obtained with HRP and TMB. The model handles the varying permeability of the beads to the peroxidase, rate constants for all of the relevant reactions, and diffusion coefficients for all of the moving species. The theory of diffusion and reaction in spherical particles is well-developed and provides the basis for our model (38). As there are 11 species to follow (Fig. 1, Table 1) we used a finite-volume numerical method to solve the balance equations simultaneously (Data Set S1).

The model reveals that diffusion rates have a relatively low impact in our system. The diffusion of HRP can be disregarded

Table 1
Reaction rate constants used in this study
Reactions to which the values apply are shown in Fig. 1.

Name	Value	Notes and references
k_1 (LP/VA)	580 mM^{-1} s^{-1}	Ref. 13
k_1 (HRP/TMB)	14,100 mM^{-1} s^{-1}	Ref. 39
k_2 (LP/VA)	90 mM^{-1} s^{-1}	Ref. 40
k_2 (HRP/TMB)	0 mM^{-1} s^{-1}	Pathway inoperative because $TMB^{+\bullet}$ is released quantitatively (35, 36)
k_3 (LP)	720 mM^{-1} s^{-1}	Calculated from extents of LP-catalyzed BODIPY bead oxidation without VA
k_3 (HRP)	1200 mM^{-1} s^{-1}	Calculated from extents of HRP-catalyzed BODIPY bead oxidation without TMB
k_4 (LP/VA)	330 mM^{-1} s^{-1}	Ref. 41
k_4 (HRP/TMB)	396 mM^{-1} s^{-1}	k_6 assumed to be rate-limiting
k_5 (LP)	0.78 s^{-1}	Calculated from rate of VA oxidation, assuming $k_5 < k_2$ (Fig. S2)
k_5 (HRP)	0 mM^{-1} s^{-1}	Pathway inoperative because $TMB^{+\bullet}$ is released quantitatively (35, 36)
k_6 (LP/VA)	10 mM^{-1} s^{-1}	Assumed to be rate-limiting in the pathway that releases $VA^{+\bullet}$ ($k_6 < k_4$). Assumed that 10% of LP turnovers involving VA proceed via this pathway (23, 40)
k_6 (HRP/TMB)	396 mM^{-1} s^{-1}	Measured from rate of TMB oxidation, assuming $k_6 < k_4$ (Fig. S1)
k_7 (LP/VA)	17 s^{-1}	Refs. 11, 21, 22
k_7 (HRP/TMB)	0.03 s^{-1}	Measured (Fig. S1)
k_8	10^6 mM^{-1} s^{-1}	Diffusion-limited
k_9	600 mM^{-1} s^{-1}	Set to give best fit of model to data

because it is preloaded into the beads. Although diffusion is a factor for H_2O_2 and TMB, because they continue to enter the beads as the peroxidase consumes them, this phenomenon has little influence on the shapes of the oxidation profiles because diffusion is rapid relative to the duration of the reaction. This is evident from the characteristic times (t) for diffusion of H_2O_2 and TMB, where $t = R^2/D$, R being the bead's radius and D being the diffusion coefficient for the substrate. The average value of R for the beads is 35 μm, whereas D is $\sim 5 \times 10^{-6}$ cm^2 s^{-1} for H_2O_2 and 3×10^{-6} cm^2 s^{-1} for TMB (42, 43). Considering just the case of TMB, the slower-moving substrate, the resulting t of 4 s indicates that within 16 s of its addition TMB arrives to 98% of the equilibrium concentration it would have in the absence of reactions that consume it (38). Likewise, the $TMB^{+\bullet}$ produced by HRP quickly attains its concentration profile within the bead, as its expected diffusion coefficient is essentially the same as that for TMB. In contrast to this rapid equilibration of all the small molecules in our system, the duration of the reaction for bead oxidation is relatively long at 6 min.

Given the relatively low impacts of diffusion rates, the oxidation profiles in the beads are governed chiefly by the rates for production and reaction of $TMB^{+\bullet}$. $TMB^{+\bullet}$ production by the peroxidase is rapid under our conditions, with a rate constant of 3.96×10^5 M^{-1} s^{-1} (Fig. S1), and obviously affects the rate of bead oxidation, but it does not affect the shapes of the profiles that appear in partially oxidized beads. Instead, the computer model reveals that the shape of the oxidation profiles is largely determined by the rates for $TMB^{+\bullet}$ reaction with the dye and for $TMB^{+\bullet}$ hydrolysis. For a given rate of reaction with the dye, a higher hydrolysis rate will result in oxidation that penetrates the bead less deeply. For a given hydrolysis rate, a higher rate of reaction with the dye will steepen the advancing front.

The relative rates at which the cation radical oxidizes the dye or hydrolyzes can be assessed by determining the apparent first-order rate constants for the two processes. Dye oxidation probably begins with a reversible outer sphere SET to $TMB^{+\bullet}$, which is expected to be a very rapid (diffusion-limited) process with a second-order rate constant around 10^9 M^{-1} s^{-1} (44). However, this initial SET cannot be the rate-limiting step. If it were, plots of fraction green *versus* radius of the beads would show abrupt oxidation fronts rather than the gradients we observed. It appears that some subsequent irreversible reaction associated with cleavage of the BODIPY 581/591-conjugated diene side chain is likely rate-limiting (30). To estimate the actual rate constant (k_9) for dye oxidation, we iteratively varied it until the model matched the observed oxidation gradients. This approach gave a value of 6×10^5 M^{-1} s^{-1} for k_9 that fits all the data (Table 1). Because the concentration of the dye in the beads was 0.5 mM, the apparent first-order rate constant for reaction of $TMB^{+\bullet}$ with the dye is then 300 s^{-1}. By contrast, the rate of $TMB^{+\bullet}$ hydrolysis as determined from our spectrophotometric observations (Fig. S1) is much lower at 0.03 s^{-1}.

These two rate constants determine that the advance of green fluorescence into the beads appears as a gradually sloped front: as long as dye molecules are available, most $TMB^{+\bullet}$ molecules react preferentially with them instead of hydrolyzing, but as more of the dye is oxidized an increasing proportion of the $TMB^{+\bullet}$ molecules is able to advance deeper into the bead. The results of the model, shown in Fig. 4*B*, generate predicted oxidation profiles that agree well with the experimental data obtained using HRP and TMB. To assess the statistical significance of this finding, we compared the positions in the experimental and modeled oxidation fronts at which the BODIPY dye was 50% oxidized. The results show that the model is within the 95% confidence intervals for the data (Fig. 4*C*).

Test of veratryl alcohol as a mediator

Because $VA^{+\bullet}$, with $E^0 = +1.36$ V in H_2O (37), is a stronger oxidant than $TMB^{+\bullet}$, the foregoing results suggested that BODIPY 581/591 immobilized within small pores should also serve as a probe to detect $VA^{+\bullet}$ if this cation radical escapes from the LP that produces it. The principal difference expected with the LP/VA system is that it would produce a less diffusible oxidation system that exhibits a sharper advancing front, because the rate constant for hydrolysis of $VA^{+\bullet}$ is 17 s^{-1} (11, 21, 22), in contrast to our observed value of 0.03 s^{-1} for $TMB^{+\bullet}$ hydrolysis (Table 1, Fig. S1). To look for evidence of VA-derived diffusible oxidants, we began by comparing the spatial distribution of oxidized dye in beads that had been oxidized by LP with and without VA. Fig. 5*A* shows representative images of the beads, and Fig. 5*B* shows the fraction of green intensity *versus* distance from the surface for replicate beads. The data show

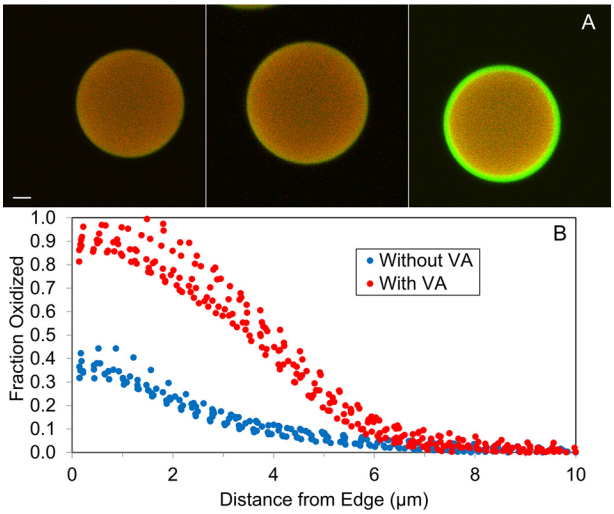

Figure 5. Imaging data for beads treated with LP, VA, and H_2O_2. *A*, confocal fluorescence images of beads exposed to the following treatments, from left to right: H_2O_2 alone (0.8 mM); LP and H_2O_2 (0.8 mM); LP, VA (12 mM), and H_2O_2 (0.8 mM). The images have been adjusted to represent constant excitation laser power. The *scale bar* is 10 μm. *B*, quantitative analyses of eight images each of beads exposed to LP and 0.8 mM H_2O_2, with and without 12 mM VA.

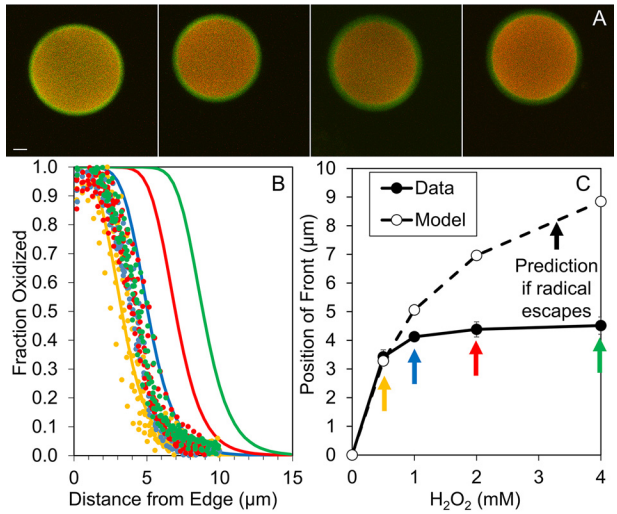

Figure 6. Imaging data for beads treated with LP and VA using increasing doses of H_2O_2. *A*, confocal fluorescence images of beads exposed to 12 mM VA and LP, using the following H_2O_2 concentrations, from left to right: 0.5, 1.0, 2.0, and 4.0 mM. The images have been adjusted to represent constant excitation laser power. The *scale bar* is 10 μm. *B*, experimental dye oxidation profiles (data points for eight replicate beads) and modeled dye oxidation profiles (*lines*) for beads treated with increasing levels of H_2O_2, using excess VA (12 mM) and LP. *Yellow*, 0.5 mM H_2O_2; *blue*, 1.0 mM H_2O_2; *red*, 2.0 mM H_2O_2; *green*, 4.0 mM H_2O_2. *C*, comparison of experimental data (*closed circles*) and reaction–diffusion model (*open circles*) for the depth into the beads at which 50% oxidation occurred after treatment with the LP/H_2O_2/VA system. Results are shown as a function of oxidant dosage, *i.e.* the amount of H_2O_2 supplied. *Error bars* on the experimental values indicate 95% confidence intervals. The *colored arrows* indicate the correspondence to the data in plot B.

that, although VA stimulated the extent of BODIPY dye oxidation at the bead periphery as expected (31), the depth of the reaction was no different with and without VA. In both cases, the extent of oxidation at a depth of 7 μm into the bead was about 5% of the extent observed at the periphery. The close correspondence between this result and the depth of labeled ovalbumin infiltration into the beads (Fig. 3) suggests that dye oxidation occurred only in the space available to LP.

However, it was necessary to consider an alternative possibility, namely that the depths of bead oxidation with and without VA were the same simply because the amount of H_2O_2 added was insufficient under our reaction conditions. Therefore, we performed additional experiments with LP in the presence of excess VA, using a series of increasing H_2O_2 concentrations. A technical difficulty with this approach is that some LP inactivation is unavoidable at high levels of H_2O_2 (45). Nevertheless, we were able to obtain progressively increasing extents of veratraldehyde production in the range of 0.5–4.0 mM H_2O_2 (Table S1). If a significant fraction of the $VA^{+\bullet}$ molecules that are precursors for this veratraldehyde can escape from the enzyme, it follows that the depth of bead oxidation should increase as the veratraldehyde yield increases.

The image analysis of beads treated according to this regime (Fig. 6, *A* and *B*) shows that oxidation initially extended deeper into the LP-accessible periphery of the beads as the H_2O_2 concentration was raised from 0.5 to 1.0 mM. However, no deeper advance of the oxidation front into the LP-inaccessible region was obtained when the H_2O_2 concentration was increased progressively to 4.0 mM, even though the veratraldehyde yields indicate that the additional H_2O_2 gave a 3.6-fold increase in the number of LP turnovers. Moreover, the final depth of oxidation appeared no greater than that obtained via direct oxidation by LP without VA in the experiment shown in Fig. 5. The only apparent change in the beads treated with the highest level of H_2O_2 was that the intensity of their peripheral green fluorescence dropped slightly, perhaps due to bleaching of the oxidized BODIPY dye via additional LP-catalyzed reactions.

This result contrasts with the data obtained using TMB as the substrate, where $TMB^{+\bullet}$ clearly acts as a diffusible mediator (Fig. 4), but the question remains as to how the oxidation profiles would appear if the $VA^{+\bullet}$ produced by LP did escape and diffuse into the beads. Specifically, is the relatively high rate of $VA^{+\bullet}$ hydrolysis by itself sufficient to explain why supplying VA did not increase the depth of bead oxidation by LP? To address this question, we applied our computer model, as it had given a good fit between data and theory for bead oxidation mediated by $TMB^{+\bullet}$. The apparent rate constant for oxidation of the BODIPY dye by $VA^{+\bullet}$ (k_9, Table 1) was taken to be the same as that for oxidation of the dye by $TMB^{+\bullet}$, because it appears that the initial SET oxidation of the dye is in any case not rate-limiting. Several other rate constants were changed to match independent experimental data that apply to $VA^{+\bullet}$ and LP (Table 1, Fig. S2), but the only one to have a large effect of the performance of the model was the $VA^{+\bullet}$ hydrolysis rate constant (k_7), which was set per the literature at 17 s^{-1} (11, 21, 22).

The model assumes that 10% of LP turnovers release $VA^{+\bullet}$ into solution, thus accounting for published results on the stoichiometry of veratraldehyde production by the enzyme (23). The results are included with the experimental data in Fig. 6*B*, and it is clear that there is a marked difference between the observed and modeled depths of oxidation. At 0.5 mM H_2O_2, the fit between the model and data is very good, which validates the value of k_9 we carried over from the HRP/TMB model. However, at higher H_2O_2 concentrations, the model indicates a continued advance of oxidation into the bead, in contrast to the

lack of deeper oxidation found experimentally. For statistical analysis, we again compared the observed and modeled positions in the advancing oxidation fronts at which the BODIPY dye was 50% oxidized (Fig. 6*C*). Although the depth of 50% oxidation increased in the LP-accessible periphery when the H_2O_2 concentration was raised from 0.5 to 1.0 mM, the data do not support deeper oxidation into the LP-inaccessible volume with increasing levels of H_2O_2. Instead, the depth of 50% oxidation appeared to approach an asymptotic value near 4.3 μm.

Discussion

VA did not enable LPA, the major isozyme of the LP H8 family (3, 32), to oxidize BODIPY 581/591 that was immobilized within beads containing pores too small for the enzyme to infiltrate. Given the marked disparity between the data and the computer simulations, the observed oxidation profiles within the beads cannot be attributed to the diffusion and reaction of $VA^{+\bullet}$. Instead, the profiles fit the progressively lower porosity that occurs with increasing depth into the beads, such that dye oxidation was possible only where LP was present. We conclude from these results that LPA does not deploy $VA^{+\bullet}$ to act as a diffusible oxidant. However, a role for $VA^{+\bullet}$ as a SET mediator that remains bound to LP continues to be a valid hypothesis, and appears consistent with our observation that VA enhanced dye oxidation by LP at the bead periphery.

A pertinent question is whether any of the other nine LPs encoded in the *P. chrysosporium* genome might employ $VA^{+\bullet}$ as a remote oxidant. A definitive answer is not yet available, because none of these isozymes were available for this study, and none have been investigated in enough mechanistic detail to obtain the kinetic constants needed for our reaction–diffusion model. However, it is worth noting that all of the LP isozymes have similar steady-state catalytic properties toward VA (46), and all display a high degree of sequence identity (Fig. S3) (3). Moreover, although computational simulations of $VA^{+\bullet}$ binding to LP have not yet been reported, comparisons of the VA-binding surface environment, which comprises 20 amino acid residues near the catalytic tryptophan residue (Trp-171 in LPA), indicate only small variations (Fig. S4) (14, 47). In particular, most of the acidic and aromatic residues that might interact with an aryl cation radical are conserved. Thus, although $VA^{+\bullet}$ in free solution is a reasonable oxidant of lignin from a chemical standpoint, the available data indicate that LPs are unlikely to produce it. Additional work with other LP isozymes is needed, but the explanation for initial attack by *P. chrysosporium* on lignin in the cell wall of sound wood probably lies elsewhere.

The best available alternative hypothesis involves sequential action by two secreted enzymes whose genes are transcribed at high levels during the growth of *P. chrysosporium* on wood: cellobiose dehydrogenase and manganese peroxidase (32). In the first step, the former enzyme reduces Fe(III), thus generating Fe(II) chelates that drive Fenton chemistry (48–50). Autoxidation of some of this Fe(II), as well as the action of fungal oxidases on secreted metabolites such as glyoxal, generate the H_2O_2 that is also required (1, 32). Because Fenton oxidation of lignin is expected to result in the *O*-demethylation of some of its aromatic rings, the polymer is predicted to become enriched in phenolic substructures (51, 52). These phenolic units, unlike the nonphenolic aryl ether units that predominate in native lignin, can be oxidatively cleaved by Mn(III) chelates, which are generated by manganese peroxidase in the second step (2, 3, 50). Although this sequence of events remains to be demonstrated for wood undergoing white rot, there is no question that the proposed reagents (Fe(II) chelates, H_2O_2, and Mn(III) chelates) are all small enough to infiltrate the wood cell wall (53).

Experimental procedures

Synthesis of dye-functionalized beads

Porous polyacrylamide beads with a nominal 6-kDa exclusion limit (Bio-Gel P-6 fine, Bio-Rad) were used. They had a mean diameter of 72 14 μm and a 48–104 μm diameter range ($n = 150$). Preparatory to BODIPY attachment, 2 g dry weight of the beads was first aminoethylated by the method of Inman and Dintzis (54). The derivatized beads were found by conductimetric titration to contain 245 μmol of NH_2 groups/g dry weight, and were stored in water/ethanol, 4:1, at 4 °C.

Aminoethylated beads (100 μl settled volume, 1.3 μmol of NH_2 groups assuming random close packing, defined as 1 eq) were transferred to an Eppendorf centrifuge filter (0.4 μm pore size) and equilibrated with 0.1 M $NaHCO_3$ (pH 8.2, 100 μl) by several cycles of low speed centrifugation (700 rpm, 1 min), with repeated addition of the $NaHCO_3$ solution. After a final centrifugation step, 0.17 eq of BODIPY 581/591 C11 SE (4,4-difluoro-5-(4-phenyl-1,3-butadienyl)-4-bora-3*a*,4*a*-diaza-*s*-indacene-3-undecanoic acid succinimidyl ester, Thermo Fisher Scientific) was added in sufficient *N*,*N*-dimethylformamide to wet the beads throughout. The mixture was allowed to react for 3 h at room temperature and then stored at 4 °C overnight. Removal of the supernatant fraction by centrifuge filtration showed that it was colorless, whereas the beads were bright red, indicating that all the dye had attached to them. The final inferred concentration of amide-linked BODIPY 581/591 in the beads was 0.5 mM.

The above derivatization procedure was then repeated using 2 eq of the succinimidyl ester of carboxyl-terminated 40-kDa polyethylene glycol monomethyl ether (Nanocs, New York). This step was included because we found that it somewhat decreased the permeability of the beads' outer surface to proteins. Finally, any remaining NH_2 groups on the beads were capped by a third cycle of derivatization with 10 eq of succinimidyl acetate (TCI America, Portland, OR), using the above procedure. The beads were rinsed with water and stored in water/ethanol, 4:1, at 4 °C.

Enzymes and reagents

HRP was Type VI from Sigma. TMB was a generous contribution from P. J. Kersten (Forest Products Laboratory, Madison, WI). VA (Sigma) was purified by vacuum distillation as described earlier (55).

LPA was expressed heterologously in *Escherichia coli* W3110. The mature protein-coding sequence of the encoding gene (GenBank™ Y00262; corresponding to LPA in the *P. chrysosporium* genome, with JGI ID 2989894) was manually curated and then synthesized by ATG:biosynthetics (Merzhausen, Germany), after checking whether all the codons had

previously been used to express other genes in *E. coli* W3110, and substituting them where required. This sequence was cloned in the expression vector pFLAG1 (International Biotechnologies, Cambridge, UK) and the resulting plasmid pFLAG1-Y00262 was directly used for expression. *E. coli* DH5α was used for plasmid propagation.

To produce the LP, cells of transformed *E. coli* W3110 were grown for 3 h in Terrific Broth (Sigma), induced with 1 mM isopropyl β-D-thiogalactopyranoside, and grown further for 4 h. The apoenzyme accumulated in inclusion bodies, as observed by SDS-PAGE, and was solubilized using 8 M urea. Subsequent *in vitro* refolding of the LP was performed using 2.1 M urea, 5 mM Ca^{2+}, 10 μM hemin, 0.7 mM oxidized glutathione, 0.1 mM dithiothreitol, and 0.2 mg ml^{-1} protein (pH 8.0) (56). Active enzyme was purified by Resource-Q chromatography (GE Healthcare), using a 0–300 mM NaCl gradient (20 min, 2 ml min^{-1} flow rate) in 10 mM sodium tartrate (pH 5.5) containing 1 mM $CaCl_2$. Previous work has shown that the kinetic properties of heterologously expressed LPA from *P. chrysosporium* are virtually the same as those of LPA isolated from the fungus (1, 41).

Enzymatic oxidations of dye-functionalized beads

Oxidations were carried out in 1-ml Eppendorf tubes at room temperature, in a final volume of 200 μl. When the role of TMB as a mediator for HRP was being investigated, complete reactions contained HRP (0.3 μM), H_2O_2 (286 μM), and fluorometric beads (16 μl settled volume) in sodium tartrate buffer (20 mM, pH 4.5). After a 1-h preincubation, the reaction was initiated with 0.71 μM TMB and the tube was mixed by continuous vortexing. At 6-min intervals, a 4-μl aliquot containing beads was withdrawn for analysis and an additional 0.71 μM TMB was added in 4 μl of water. Spectrophotometric monitoring at 450 nm of a parallel reaction without beads indicated that 6 min was sufficient to reach an end point after each addition of TMB, *i.e.* that production of the TMB cation radical ($TMB^{+\bullet}$) had ceased before this time (Fig. S1) (35, 36). We used limiting TMB in these experiments because the low quantity of oxidant necessary for bead oxidation dictated that the limiting substrate had to be added at a low concentration, and this would have been difficult with the needed accuracy using H_2O_2, because dilute solutions of it are susceptible to reaction with trace metals.

When the role of TMB or VA as a mediator for LP was being investigated, complete reactions (200 μl in Eppendorf tubes) contained LP (3 μM), TMB (4 mM), or VA (12 mM), and fluorometric beads (3 μl settled volume) in sodium tartrate buffer (20 mM, pH 4.5). After a 1-h preincubation, the reactions were initiated with H_2O_2 (0.1–4.0 mM) and the tubes were continuously mixed by vortexing for 30 min. Spectrophotometric monitoring at 310 nm of parallel reactions without beads indicated that the reactions had reached an end point before this time, *i.e.* that veratraldehyde production had ceased (Fig. S2) (51). We used limiting H_2O_2 in these experiments because the relatively high quantity of oxidant necessary for bead oxidation dictated that the nonlimiting substrate had to be added at a concentration much higher than 1 mM. Because LP is inactivated by millimolar concentrations of H_2O_2, and donor substrates such as VA partially protect the enzyme against this inactivation (45), a design using excess electron donor appeared most prudent.

Imaging of beads

Confocal imaging was done on a Zeiss 510 Meta confocal laser scanning microscope, using a 1.2 numerical aperture ×40 water objective. Samples were in water at 20 °C. Images were acquired using the unit's integral camera, in 2-μm thick optical sections and a pixel width of 0.11 μm. Red emission due to native BODIPY dye was collected with a 560-nm long pass filter and 543 nm excitation, and green emission due to oxidized dye was collected at 500–550 nm with 488 nm excitation. Laser power was adjusted for each image to use the full dynamic range of the photomultiplier tube detectors. Images were processed using Zeiss LSM software. Fluorescence resonance transfer (FRET) between dye molecules in the beads was not a technical concern in this study because the concentration of attached BODIPY (0.5 mM) corresponds to an average intermolecular distance greater than 100 Å, which exceeds the 30–60 Å distance over which significant FRET can occur (57).

Measurements of ovalbumin infiltration into beads

Fluorescein-labeled ovalbumin (Thermo Fisher Scientific) was dissolved in sodium borate buffer (200 mM, pH 8.0) at a concentration of 1 mg/ml. A portion (8 μl) of this solution was combined with BODIPY-functionalized beads (2 μl settled volume) and observed at 3-min intervals by confocal microscopy as described above for bead oxidation experiments, the only difference being that in this case the green emission was due to labeled ovalbumin rather than to oxidized BODIPY. The final images were acquired at 90 min, when it was clear that ovalbumin movement into the beads had ceased.

Image analysis

Images were processed using Python 2.7 scripts, based on functions in the OpenCV module, version 2.4.10 (www.opencv.org).[5] The script is available in Data Set S1. For experiments on BODIPY dye oxidation, the edge of the bead was found by selecting a threshold value near 20% of the maximum fluorescence intensity, and then applying it to a gray-scale composite image. This approach leads to an uncertainty of less than 0.25 μm in the position of the edge. The beads were then isolated using a contouring routine. Beads that touched the edge of the image or another bead were excluded from the analysis. From the contour, the centroid of the bead was determined. The pixels 2 to 5 μm outside the bead were used to determine the background emission for each color, and these background values were subtracted from the respective channels. Next, because a range of laser powers had been used to acquire the images, the apparent intensities of all images were adjusted to bring all the data to constant laser power. Finally, the average fraction of green intensity was tallied for all the pixels in a series of annular disks centered on the centroid of the beads. These data are presented as fraction of green *versus* distance from the center of the beads.

[5] Please note that the JBC is not responsible for the long-term archiving and maintenance of this site or any other third party hosted site.

In the case of the fluorescein-labeled ovalbumin experiments, we defined the bead edge as the location at which the red channel fluorescence intensity due to native BODIPY dye was 50% of the background intensity in the surrounding solution. This approach leads to an uncertainty of less than 0.25 μm in the position of the edge.

Computer modeling

Reaction–diffusion modeling of the beads was accomplished using Python 2.7 and the FiPy 3.1 module (https://www.ctcms.nist.gov/fipy/) (58), which is an implementation of the finite volume method for solving time-dependent partial differential equations (Data Set S1). Because the beads are spherical, the mathematical model reduces to a time-dependent, one-dimensional set of equations. The chemical reactions allowed are shown in Fig. 1, and relevant rate constants are shown in Table 1. The reaction–diffusion model followed 11 species during the course of the reactions: E_o, ferric resting state peroxidase; O=E_i, two-electron-oxidized peroxidase compound I; HO-E_{ii}, one-electron-oxidized peroxidase compound II; HO-E_{ii}-$M^{+\bullet}$, peroxidase compound II associated with mediator cation radical; M =≥mediator (TMB or VA); $M^{+\bullet}$ =≥mediator cation radical; A, two-electron-oxidized product derived from mediator (2,5-dimethoxybenzoquinone or veratraldehyde); R, native red BODIPY dye; G, oxidized green BODIPY dye; H_2O_2; and $HO_2^{\bullet}$. As indicated in Fig. 1, $HO_2^{\bullet}$ production, although expected at some level following VA oxidation (23, 24), is not associated with TMB oxidation. Therefore, $HO_2^{\bullet}$ production was preset to 0 when TMB oxidation was modeled.

Because the BODIPY dye was covalently attached to the beads and the peroxidases were pre-equilibrated with them before the reactions, only M, $M^{+\bullet}$, H_2O_2, and $HO_2^{\bullet}$ were allowed to diffuse in the model. The diffusion coefficient (D) used for H_2O_2 was the measured literature value (5×10^{-6} cm^2 s^{-1}) (43), and D for the similarly sized $HO_2^{\bullet}$ molecule was assumed to be the same. The value of D for M and $M^{+\bullet}$ was assumed to be the same as reported earlier for similarly sized aromatic molecules in water (3×10^{-6} cm^2 s^{-1}) (42). For purposes of the model, the boundary condition at the surface was set to values obtained from a solution phase model assuming that the liquid phase was well-mixed. The solution phase model resulted in a set of ordinary differential equations that were solved using the "Integrate" functions in the SciPy module (Data Set S1). Consistent with the spherical symmetry, the boundary condition at the center was the gradient with distance set to zero.

Although the BODIPY dye was not allowed to diffuse in the model, its concentration was allowed to vary across the bead, being set to match measured values that were determined by image analysis of the control beads. In this way, the model took account of the fact that the concentration of attached dye was slightly higher at the bead periphery than at its center. Likewise, although the peroxidase was not allowed to diffuse in the model, its concentration across the bead was allowed to vary, being set to match the profiles of bead oxidation that we observed when LP was used to oxidize the beads directly without a mediator. That is, the shape of the gradient in dye oxidation was taken to indicate the shape of the gradient in peroxidase infiltration, this approach being feasible because the dye was only partially oxidized, even at the outmost edge of the bead, in experiments without mediator. We used these measurements of dye oxidation as a reporter for peroxidase location because the results were essentially unaffected by background fluorescence, as opposed to the data from measurements of infiltration using fluorescently labeled ovalbumin, which contained signal from the high concentration of labeled ovalbumin that was present in the buffer surrounding the beads.

Author contributions—C. J. H. and K. E. H. conceptualization; C. J. H., C. G. H., A. T. M., and K. E. H. resources; C. J. H., E. M., C. G. H., E. F.-F., A. T. M., and K. E. H. data curation; C. J. H. software; C. J. H., E. M., C. G. H., and E. F.-F. formal analysis; C. J. H., A. T. M., and K. E. H. supervision; C. J. H., C. G. H., and K. E. H. funding acquisition; C. J. H., E. M., C. G. H., E. F.-F., A. T. M., and K. E. H. validation; C. J. H., E. M., C. G. H., E. F.-F., A. T. M., and K. E. H. investigation; C. J. H., E. M., C. G. H., E. F.-F., and A. T. M. visualization; C. J. H., E. M., C. G. H., E. F.-F., A. T. M., and K. E. H. methodology; C. J. H., E. M., and K. E. H. writing-original draft; C. J. H., C. G. H., and K. E. H. project administration; C. J. H., C. G. H., E. F.-F., A. T. M., and K. E. H. writing-review and editing.

References

1. Fernández-Fueyo, E., Ruiz-Dueñas, F. J., Ferreira, P., Floudas, D., Hibbett, D. S., Canessa, P., Larrondo, L. F., James, T. Y., Seelenfreund, D., Lobos, S., Polanco, R., Tello, M., Honda, Y., Watanabe, T., Watanabe, T., *et al.* (2012) Comparative genomics of *Ceriporiopsis subvermispora* and *Phanerochaete chrysosporium* provide insight into selective ligninolysis. *Proc. Natl. Acad. Sci. U.S.A.* **109,** 5458–5463 CrossRef Medline
2. Hammel, K. E., and Cullen, D. (2008) Role of fungal peroxidases in biological ligninolysis. *Curr. Opin. Plant. Biol.* **11,** 349–355 CrossRef Medline
3. Martínez, A. T. (2002) Molecular biology and structure-function of lignin-degrading heme peroxidases. *Enzyme Microb. Technol.* **30,** 425–444 CrossRef
4. Floudas, D., Binder, M., Riley, R., Barry, K., Blanchette, R. A., Henrissat, B., Martínez, A. T., Otillar, R., Spatafora, J. W., Yadav, J. S., Aerts, A., Benoit, I., Boyd, A., Carlson, A., Copeland, A., *et al.* (2012) The paleozoic origin of enzymatic lignin decomposition reconstructed from 31 fungal genomes. *Science* **336,** 1715–1719 CrossRef Medline
5. Nagy, L. G., Riley, R., Tritt, A., Adam, C., Daum, C., Floudas, D., Sun, H., Yadav, J. S., Pangilinan, J., Larsson, K. H., Matsuura, K., Barry, K., Labutti, K., Kuo, R., Ohm, R. A., *et al.* (2016) Comparative genomics of early-diverging mushroom-forming fungi provides insights into the origins of lignocellulose decay capabilities. *Mol. Biol. Evol.* **33,** 959–970 CrossRef Medline
6. Blanchette, R. A., Burnes, T. A., Eerdmans, M. M., and Akhtar, M. (1992) Evaluating isolates of *Phanerochaete chrysosporium* and *Ceriporiopsis subvermispora* for use in biological pulping processes. *Holzforschung* **46,** 109–115 CrossRef
7. Blanchette, R. A., Krueger, E. W., Haight, J. E., Akhtar, M., and Akin, D. E. (1997) Cell wall alterations in loblolly pine wood decayed by the white-rot fungus, *Ceriporiopsis subvermispora*. *J. Biotechnol.* **53,** 203–213 CrossRef
8. Camarero, S., Sarkar, S., Ruiz-Dueñas, F. J., Martínez, M. J., and Martínez, A. T. (1999) Description of a versatile peroxidase involved in the natural degradation of lignin that has both manganese peroxidase and lignin peroxidase substrate interaction sites. *J. Biol. Chem.* **274,** 10324–10330 CrossRef Medline
9. Mester, T., and Field, J. A. (1998) Characterization of a novel manganese peroxidase-lignin peroxidase hybrid isozyme produced by *Bjerkandera* species strain BOS55 in the absence of manganese. *J. Biol. Chem.* **273,** 15412–15417 CrossRef Medline
10. Paszczyński, A., Huynh, V. B., and Crawford, R. (1986) Comparison of ligninase-1 and peroxidase-M2 from the white-rot fungus *Phanerochaete chrysosporium*. *Arch. Biochem. Biophys.* **244,** 750–765 CrossRef Medline

11. Candeias, L. P., and Harvey, P. J. (1995) Lifetime and reactivity of the veratryl alcohol radical cation: implications for lignin peroxidase catalysis. *J. Biol. Chem.* **270,** 16745–16748 CrossRef Medline
12. Harvey, P. J., Schoemaker, H. E., and Palmer, J. M. (1986) Veratryl alcohol as a mediator and the role of radical cations in lignin biodegradation by *Phanerochaete chrysosporium*. *FEBS Lett.* **195,** 242–246 CrossRef
13. Tien, M., Kirk, T. K., Bull, C., and Fee, J. A. (1986) Steady-state and transient-state kinetic studies on the oxidation of 3,4-dimethoxybenzyl alcohol catalyzed by the ligninase of *Phanerochaete chrysosporium* Burds. *J. Biol. Chem.* **261,** 1687–1693 Medline
14. Acebes, S., Ruiz-Dueñas, F. J., Toubes, M., Sáez-Jiménez, V., Pérez-Boada, M., Lucas, M. F., Martínez, A. T., and Guallar, V. (2017) Mapping the long-range electron transfer route in ligninolytic peroxidases. *J. Phys. Chem. B* **121,** 3946–3954 CrossRef Medline
15. Sáez-Jiménez, V., Baratto, M. C., Pogni, R., Rencoret, J., Gutiérrez, A., Santos, J. I., Martínez, A. T., and Ruiz-Dueñas, F. J. (2015) Demonstration of lignin-to-peroxidase direct electron transfer: a transient-state kinetics, directed mutagenesis, EPR, and NMR study. *J. Biol. Chem.* **290,** 23201–23213 CrossRef Medline
16. Sáez-Jiménez, V., Rencoret, J., Rodríguez-Carvajal, M. A., Gutiérrez, A., Ruiz-Dueñas, F. J., and Martínez, A. T. (2016) Role of surface tryptophan for peroxidase oxidation of nonphenolic lignin. *Biotechnol. Biofuels* **9,** 198 CrossRef
17. Hammel, K. E., Kalyanaraman, B., and Kirk, T. K. (1986) Substrate free radicals are intermediates in ligninase catalysis. *Proc. Natl. Acad. Sci. U.S.A.* **83,** 3708–3712 CrossRef Medline
18. Kirk, T. K., Tien, M., Kersten, P. J., Mozuch, M. D., and Kalyanaraman, B. (1986) Ligninase of *Phanerochaete chrysosporium*: mechanism of its degradation of the nonphenolic arylglycerol-β-aryl ether substructure of lignin. *Biochem. J.* **236,** 279–287 CrossRef Medline
19. de Jong, E., Field, J. A., and de Bont, J. A. (1994) Aryl alcohols in the physiology of ligninolytic fungi. *FEMS Microbiol. Rev.* **13,** 153–188 CrossRef
20. Khindaria, A., Grover, T. A., and Aust, S. D. (1995) Evidence for formation of the veratryl alcohol cation radical by lignin peroxidase. *Biochemistry* **34,** 6020–6025 CrossRef Medline
21. Baciocchi, E., Bietti, M., Gerini, M. F., and Lanzalunga, O. (2002) The mediation of veratryl alcohol in oxidations promoted by lignin peroxidase: the lifetime of veratryl alcohol radical cation. *Biochem. Biophys. Res. Commun.* **293,** 832–835 CrossRef Medline
22. Bietti, M., Baciocchi, E., and Steenken, S. (1998) Lifetime, reduction potential and base-induced fragmentation of the veratryl alcohol radical cation in aqueous solution. Pulse radiolysis studies on a ligninase "mediator". *J. Phys. Chem. A* **102,** 7337–7342 CrossRef
23. Bono, J. J., Goulas, P., Boe, J. F., Portet, N., and Seris, J. L. (1990) Effect of Mn(II) on reactions catalyzed by lignin peroxidase from *Phanerochaete chrysosporium*. *Eur. J. Biochem.* **192,** 189–193 CrossRef
24. Hammel, K. E., Tien, M., Kalyanaraman, B., and Kirk, T. K. (1985) Mechanism of oxidative C_{α}-C_{β} cleavage of a lignin model dimer by *Phanerochaete chrysosporium* ligninase: stoichiometry and involvement of free radicals. *J. Biol. Chem.* **260,** 8348–8353 Medline
25. Goodwin, D. C., Aust, S. D., and Grover, T. A. (1995) Evidence for veratryl alcohol as a redox mediator in lignin peroxidase-catalyzed oxidation. *Biochemistry* **34,** 5060–5065 CrossRef Medline
26. Koduri, R. S., and Tien, M. (1995) Oxidation of guaiacol by lignin peroxidase: role of veratryl alcohol. *J. Biol. Chem.* **270,** 22254–22258 CrossRef Medline
27. Tien, M., and Ma, D. (1997) Oxidation of 4-methoxymandelic acid by lignin peroxidase: mediation by veratryl alcohol. *J. Biol. Chem.* **272,** 8912–8917 CrossRef Medline
28. Hammel, K. E., Jensen, K. A., Jr., Mozuch, M. D., Landucci, L. L., Tien, M., and Pease, E. A. (1993) Ligninolysis by a purified lignin peroxidase. *J. Biol. Chem.* **268,** 12274–12281 Medline
29. Khindaria, A., Yamazaki, I., and Aust, S. D. (1996) Stabilization of the veratryl alcohol cation radical by lignin peroxidase. *Biochemistry* **35,** 6418–6424 CrossRef Medline
30. Drummen, G. P., Gadella, B. M., Post, J. A., and Brouwers, J. F. (2004) Mass spectrometric characterization of the oxidation of the fluorescent lipid peroxidation reporter molecule C11-BODIPY 581/591. *Free Radic. Biol. Med.* **36,** 1635–1644 CrossRef Medline
31. Hunt, C. G., Houtman, C. J., Jones, D. C., Kitin, P., Korripally, P., and Hammel, K. E. (2013) Spatial mapping of extracellular oxidant production by a white rot basidiomycete on wood reveals details of ligninolytic mechanism. *Environ. Microbiol.* **15,** 956–966 CrossRef Medline
32. Korripally, P., Hunt, C. G., Houtman, C. J., Jones, D. C., Kitin, P. J., Cullen, D., and Hammel, K. E. (2015) Regulation of gene expression during the onset of ligninolytic oxidation by *Phanerochaete chrysosporium* on spruce wood. *Appl. Environ. Microbiol.* **81,** 7802–7812 CrossRef Medline
33. Dimonie, M. V., Boghina, C. M., Marinescu, N. N., Marinescu, M. M., Cincu, C. I., and Oprescu, C. G. (1982) Inverse suspension polymerization of acrylamide. *Eur. Polym. J.* **18,** 639–645 CrossRef
34. Gorrebeeck, C., Spanoghe, M., Lanens, D., Lemiere, G. L., Dommisse, R. A., Lepoivre, J. A., and Alderweireldt, F. C. (1991) Permeability studies on horse liver alcohol dehydrogenase (HLAD) in polyacrylamide gel beads. *Recl. Trav. Chim. Pays-Bas* **110,** 231–235 CrossRef
35. Kersten, P. J., Kalyanaraman, B., Hammel, K. E., Reinhammar, B., and Kirk, T. K. (1990) Comparison of lignin peroxidase, horseradish peroxidase and laccase in the oxidation of methoxybenzenes. *Biochem. J.* **268,** 475–480 CrossRef Medline
36. Koduri, R. S., Whitwam, R. E., Barr, D., Aust, S. D., and Tien, M. (1996) Oxidation of 1,2,4,5-tetramethoxybenzene by lignin peroxidase of *Phanerochaete chrysosporium*. *Arch. Biochem. Biophys.* **326,** 261–265 CrossRef
37. Branchi, B., Galli, C., and Gentili, P. (2005) Kinetics of oxidation of benzyl alcohols by the dication and radical cation of ABTS: comparison with laccase-ABTS oxidations: an apparent paradox. *Org. Biomol. Chem.* **3,** 2604–2614 CrossRef Medline
38. Cussler, E. L. (1984) *Diffusion: Mass Transfer in Fluid Systems*, Cambridge University Press, Cambridge
39. Dolman, D., Newell, G. A., and Thurlow, M. D. (1975) A kinetic study of the reaction of horseradish peroxidase with hydrogen peroxide. *Can. J. Biochem.* **53,** 495–501 CrossRef Medline
40. Harvey, P. J., Palmer, J. M., Schoemaker, H. E., Dekker, H. L., and Wever, R. (1989) Pre-steady-state kinetic study on the formation of Compound I and II of ligninase. *Biochim. Biophys. Acta* **994,** 59–63 CrossRef Medline
41. Khindaria, A., Yamazaki, I., and Aust, S. D. (1995) Veratryl alcohol oxidation by lignin peroxidase. *Biochemistry* **34,** 16860–16869 CrossRef Medline
42. Niesner, R., and Heintz, A. (2000) Diffusion coefficients of aromatics in aqueous solution. *J. Chem. Eng. Data* **45,** 1121–1124 CrossRef
43. van Stroe-Biezen, S. A. M., Everaerts, F. M., Janssen, L. J. J., and Tacken, R. A. (1993) Diffusion coefficients of oxygen, hydrogen peroxide and glucose in a hydrogel. *Anal. Chim. Acta* **273,** 553–560 CrossRef
44. Goez, M., and Eckert, G. (1991) Flash CIDNP study of photosensitized electron transfer reactions of methoxybenzenes. *Ber. Bunsenges. Phys. Chem.* **95,** 1179–1186 CrossRef
45. Cai, D., and Tien, M. (1992) Kinetic studies on the formation and decomposition of compound II and compound III: reactions of lignin peroxidase with H_2O_2. *J. Biol. Chem.* **267,** 11149–11155 Medline
46. Farrell, R. L., Murtagh, K. E., Tien, M., Mozuch, M. D., and Kirk, T. K. (1989) Physical and enzymatic properties of lignin peroxidase isozymes from *Phanerochaete chrysosporium*. *Enzyme Microb. Technol.* **11,** 322–329 CrossRef
47. Recabarren, R., Fuenzalida-Valdivia, I., and Alzate-Morales, J. (2016) Studying the binding mechanisms of veratryl alcohol to *P. chrysosporium* lignin peroxidase: insights from theoretical approaches. *Theor. Chem. Acc.* **135,** 1–12 CrossRef
48. Forney, L. J., Reddy, C. A., Tien, M., and Aust, S. D. (1982) The involvement of hydroxyl radical derived from hydrogen peroxide in lignin degradation by the white rot fungus *Phanerochaete chrysosporium*. *J. Biol. Chem.* **257,** 11455–11462 Medline
49. Kremer, S. M., and Wood, P. M. (1992) Evidence that cellobiose oxidase from *Phanerochaete chrysosporium* is primarily an Fe(III) reductase: kinetic comparison with neutrophil NADPH oxidase and yeast flavocytochrome B2. *Eur. J. Biochem.* **205,** 133–138 CrossRef Medline
50. Hildén, L., Johansson, G., Pettersson, G., Li, J., Ljungquist, P., and Henriksson, G. (2000) Do the extracellular enzymes cellobiose dehydrogenase

and manganese peroxidase form a pathway in lignin biodegradation? *FEBS Lett.* **477,** 79–83 CrossRef Medline
51. Urano, Y., Higuchi, T., and Hirobe, M. (1996) Substrate-dependent changes of the oxidative *O*-dealkylation mechanism of several chemical and biological oxidizing systems. *J. Chem. Soc. Perkin Trans.* **2,** 1169–1173 CrossRef
52. Filley, T. R., Cody, G. D., Goodell, B., Jellison, J., Noser, C., and Ostrofsky, A. (2002) Lignin demethylation and polysaccharide decomposition in spruce sapwood degraded by brown rot fungi. *Org. Geochem.* **33,** 111–124 CrossRef
53. Stone, J. E., and Scallan, A. M. (1968) A structural model for the cell wall of water-swollen wood pulp fibers based on their accessibility to macromolecules. *Cellulose Chem. Technol.* **2,** 343–358
54. Inman, J. K., and Dintzis, H. M. (1969) Derivatization of cross-linked polyacrylamide beads: controlled introduction of functional groups for preparation of special-purpose, biochemical adsorbents. *Biochemistry* **8,** 4074–4082 CrossRef Medline
55. Tien, M., and Kirk, T. K. (1988) Lignin peroxidase of *Phanerochaete chrysosporium*. *Methods Enzymol.* **161,** 238–249 CrossRef
56. Doyle, W. A., and Smith, A. T. (1996) Expression of lignin peroxidase H8 in *Escherichia coli*: folding and activation of the recombinant enzyme with Ca^{2+} and haem. *Biochem. J.* **315,** 15–19 CrossRef Medline
57. Lakowicz, J. R. (1983) *Principles of Fluorescence Spectroscopy*, Plenum Press, New York
58. Guyer, J. E., Wheeler, D., and Warren, J. A. (2009) FiPy: partial differential equations with python. *Comp. Sci. Eng.* **11,** 6–15 CrossRef

Fungal lignin peroxidase does not produce the veratryl alcohol cation radical as a diffusible ligninolytic oxidant

Carl J. Houtman, Eranda Maligaspe, Christopher G. Hunt, Elena Fernández-Fueyo, Angel T. Martínez and Kenneth E. Hammel

J. Biol. Chem. 2018, 293:4702-4712.
doi: 10.1074/jbc.RA117.001153 originally published online February 9, 2018